Eur. Phys. J. B **28**, 243–251 (2002)
DOI: 10.1140/epjb/e2002-00226-6

THE EUROPEAN PHYSICAL JOURNAL B

A shell-model approach to fractal-induced turbulence

B. Mazzi[1,a], F. Okkels[2], and J.C. Vassilicos[3,b]

[1] DAMTP, University of Cambridge, Cambridge CB3 9 EW, UK
[2] OFD, Risø National Laboratory and CATS, Niels Bohr Institute, University of Copenhagen, Copenhagen, Danemark
[3] Dept. of Aeronautics, Imperial College London, London, UK

Received 25 June 2001 / Received in final form 5 April 2002
Published online 19 July 2002 –

Abstract. We present a shell-model of fractal induced turbulence which predicts that structure function scaling exponents decrease in absolute value as the fractal dimension of the turbulence-inducing fractal object increases. This qualitative prediction is in agreement with laboratory measurements. Finer details of the fractal induced turbulence statistics and dynamics depend on the fractal force's phases, *i.e.* on the detailed construction of the fractal stirrer. In a case of deterministic forcing phases, a critical fractal dimension exists below which the average rate of inter-scale energy transfer $\langle T_n \rangle$ is a decreasing function of the wavenumber k_n and the structure function scaling exponents take close to Kolmogorov values. Above this critical fractal dimension, $\langle T_n \rangle$ is an increasing function of k_n and the structure function scaling exponents deviate significantly from Kolmogorov values.

PACS. 47.27.Ak Fundamentals – 47.27.Gs Isotropic turbulence; homogeneous turbulence

1 Introduction

Turbulence has a multiple scale structure and many theories and geometrical models of turbulence have in fact assumed the turbulence to be of fractal or spiral nature [1–4]. This inspired a new experimental setup where the turbulence is forced by a 3-D fractal grid. It was found that a change in the fractal dimension of the grid alters the scaling of the structure functions of the turbulence generated by the fractal grid [5].

In this paper we force a shell-model of turbulence in a way equivalent to the forcing generated by the fractal object in the laboratory experiment. Shell-models are reduced models of Navier-Stokes turbulence and they simulate the flow of energy among different wave-numbers in fully developed turbulence.

A brief description of the experiment and its fractal forcing is introduced in the next section. The shell-model used and its scale-invariant forcing are introduced in Sections 3 and 4. The numerical results are presented in Sections 5 and 6, and we conclude with a discussion in Section 7.

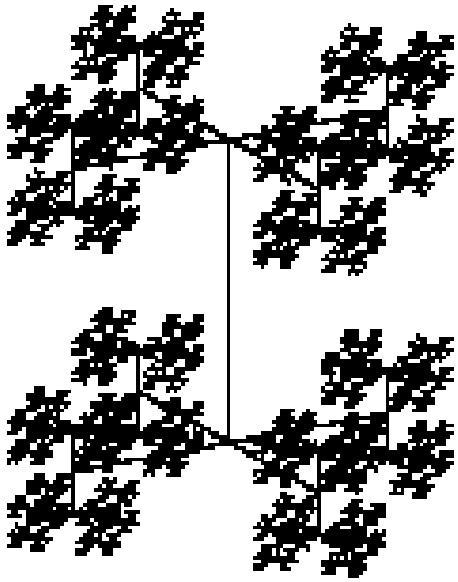

Fig. 1. The fractal object.

2 Fractal forcing in the laboratory

Measurements of fractal induced turbulence were conducted by Queiros-Conde and Vassilicos [5] and a detailed description of the apparatus and the equipment can be found in [5]. Four fractal objects of fractal dimensions

[a] e-mail: b.mazzi@damtp.cam.ac.uk
[b] e-mail: j.c.vassilicos@ic.ac.uk

$D_1 = 2.05$, $D_2 = 2.17$, $D_3 = 2.40$, $D_4 = 2.75$ were placed in the wind tunnel. A schematic picture of the actual object is given in Figure 1.

The objects were obtained by iterating the pattern of a combined double-cross with similar crosses placed at its eight ends (see Fig. 1). The ratios between successive characteristic lengths in the iteration were, respectively for each of the four fractal objects: $R_1 = 0.36$, $R_2 = 0.4$, $R_3 = 0.45$, $R_4 = 0.5$. Constraints on the number of possible iterations were set by the size of the wind tunnel and the smallest scale of the fractal objects, which was about 2 mm. Hence for three of the objects the pattern was iterated four times, whereas for the one with fractal dimension $D_4 = 2.75$ it was iterated five times.

When turbulence is created by forcing a certain flow, *e.g.* with an obstacle, the forcing is usually confined at a particular large length scale. By using a fractal object, however, we force the flow over a wide range of length-scales simultaneously from the largest to the smallest in the fractal structure. In the course of the study of turbulence, particularly since the 1960s, numerous models and approaches have assumed that turbulence is effectively a fractal phenomenon and great attention has been paid to the scaling of structure functions as a function of some fractal dimension of the flow [1–3,5,6]. Applying a fractal forcing to the flow is directly addressing the heart of the matter which is the multiscale structure of the turbulence on which the relation between the kinetic energy dissipation of the turbulence and the Reynolds number crucially depends. Hence by acting on the multiscale structure of the turbulence itself we may expect the scalings of structure functions to be affected.

3 The GOY shell-model

All shell-models simulate the flow of energy through wavenumber space in fully developed turbulence. The dynamics of the models are determined by a system of coupled ordinary differential equations where energy is injected into some of the wave-numbers by a time-independent forcing term. The energy is transported across wave-numbers by means of a coupling term and is dissipated away by a viscosity term at the high wave-numbers.

3.1 Construction

Unlike direct numerical simulations of the Navier-Stokes equations, shell-models are based on assumptions which reduce the number of free variables.

Firstly, wave-number space is divided into a set of N spherical shells of wave-number $k_n = k_0\lambda^n \quad n = 1, \ldots, N$ where λ is the ratio between successive shells (normally set equal to 2) and k_0 is a constant determining the smallest wavenumber in the model. Each shell is assigned a single complex velocity amplitude u_n. The absolute value of u_n is often thought of as a velocity difference across the length-scale $\ell_n = 1/k_n$ in the turbulent flow-field.

Secondly, using additional assumptions of conservation of phase space and energy and locality of direct interactions among shells (nearest and next nearest) one can obtain the GOY-model set of evolution equations [7–10]

$$\left(\frac{\mathrm{d}}{\mathrm{d}t} + \nu k_n^2\right) u_n = \mathrm{i}k_n(u_{n+1}^* u_{n+2}^* - \frac{\delta}{2}u_{n-1}^* u_{n+1}^* - \frac{1-\delta}{4}u_{n-2}^* u_{n-1}^*) + f_n \qquad (1)$$

with a forcing $f_n \equiv f(k_n)$ on the shells. The set (Eq. (1)) of N coupled ordinary differential equations is numerically integrated by standard techniques [12]. In the simulations we use the following standard values: $N = 19$, $\nu = 10^{-6}$, $k_0 = 2^{-4}$. The parameter δ controls the transition between the different dynamics of the model, going from a constant solution to limit cycle, torus and at the end a chaotic behaviour as δ is increased [10]. The demand of helicity conservation implies $\delta = \frac{1}{2}$, which is the standard value for the GOY shell-model [9].

3.2 Conservation laws, fixed points and invariance

Shell-models are by construction simpler than the Navier-Stokes equations but they possess the same conservation-laws. In the GOY-model, as is the case for other shell-models, these conservation laws are strictly valid in the absence of forcing and viscosity ($f = 0, \nu = 0$).

There is conservation of phase-space because the coupling term does not contain u_n, and the other conserved quantities are quadratic *i.e.* they can be written in the form: $Q_\alpha = \sum k_n^\alpha |u_n|^2$. Using the relation $\frac{1}{2}(\dot{u_n^2}) = u_n \dot{u}_n$ to derive an equation for Q_α from equation (1), leads to conservation of Q_α for $f = 0$ and $\nu = 0$ when $1 - \delta 2^\alpha - (1-\delta)2^{2\alpha} = 0$ This condition has two solutions: $\alpha = 0$ and $\alpha = -\ln_\lambda(\delta - 1)$. The first ($\alpha = 0$) corresponds to energy-conservation while the other solution corresponds to helicity conservation in the case of three dimensional turbulence ($\delta < 1$) and to enstrophy conservation in the case of two dimensional turbulence ($\delta > 1$) [9,11,12].

4 Fractal forcing in the GOY shell-model

In the standard GOY-model, the forcing is time independent and applied to one of the lowest wavenumber shells (most frequently the fourth one). With such forcing the model reproduces the Richardson cascade of turbulence whereby the energy is fed into the low wave-numbers, cascades up the inertial subrange of wavenumbers and is then dissipated away by viscosity at the largest wave-numbers [13].

To simulate the forcing of a fractal object producing turbulence in a flow, we force every single shell of the GOY-model equation given by equation (1). To respect the scaling-invariance of the fractal, the forcing is taken to vary as a power-law of wave-number, *i.e.*

$$f_n \sim {k_n}^\beta. \qquad (2)$$

4.1 Relation between R and β

The fractal dimension of the fractal object is determined by only one parameter which is the ratio R between length scales in successive iterations of the fractal construction (see Fig. 1). Characteristic lengths of crosses at iteration n are given by:

$$L_n = R^n L_0 \tag{3}$$

and the diameters of the rods that these crosses are made of are determined by the same ratio, *i.e.* $D_n = R^n D_0$.

We assume that the force f_n at length-scale L_n is proportional to the drag on structures of that length-scale, and we also assume that the total drag is proportional to the total surface. We therefore need to calculate the total surface $S(L_n)$ of structures characterised by length-scale L_n. This calculation leads to an overestimate of the total drag force, but may be a sufficiently good estimate in the limit of very small aspect ratios D_0/L_0.

This total surface is proportional to the total number of rods at a given iteration n (there are 4 rods per cross, *i.e.* 8 per double cross) times the surface of a rod of length-scale L_n (see Appendix in [5]) *i.e.*

$$S_n = 4L_0D_0\left(\frac{1}{R}+R\right)\left(8R^2\right)^n \sim \left(8R^2\right)^n \sim f_n. \tag{4}$$

Using equation (3) in conjunction with equation (4) leads to

$$f_n \sim \exp\!\big((\ln 8 + 2\ln R)\,\tfrac{\ln \ell}{\ln R}\big) = L_n^{\frac{\ln 8}{\ln R}+2}. \tag{5}$$

Let us replace L_n by k_n^{-1} in equation (5); we obtain $f_n \sim k_n^{-\left(\frac{\ln 8}{\ln R}+2\right)}$ and comparing with equation (2) gives

$$\beta = -\left(3\frac{\ln 2}{\ln R}+2\right). \tag{6}$$

Note that because $0 \le R \le 1/2$, β has to be within the range $-2 \le \beta \le 1$. The relation between R and D_f is detailed in [5], and for the fractal objects used in [5], the correspondence between R, D_f and β is as follows:

R	D_f	β
0.36	2.05	0.035
0.4	2.17	0.27
0.45	2.4	0.60
0.5	2.75	1.0

4.2 Simple relations between α and β

We now consider power law solutions $u_n \sim k_n^\alpha$ and obtain a relation between α and β from a consideration concerning the energy flux through a shell n. As for the Navier-Stokes equations [14] a *scale-by-scale energy budget equation* can also be obtained for shell-models. In the present case of the GOY model, this scale by scale energy budget is derived from equation (1) and reads

$$\frac{\partial E_n}{\partial t} + T_n = -2\nu\Omega_n + \frac{1}{2}\left(f_n u_n^* + f_n^* u_n\right) \tag{7}$$

where

$$E_n \equiv \frac{1}{2}|u_n|^2, \tag{8}$$

$$\Omega_n \equiv \frac{1}{2}k_n^2|u_n|^2 \tag{9}$$

and [15]

$$T_n = -\Im\left[k_n u_n u_{n+1}\left(u_{n+2} - \frac{\delta}{2}u_{n-1}\right) - k_n u_n \frac{1-\delta}{4}u_{n-2}u_{n-1}\right]. \tag{10}$$

Statistical stationarity in time requires

$$\frac{\partial\langle E_n\rangle}{\partial t} = 0 \tag{11}$$

where the brackets denote a statistical average (in Sect. 5 we explain how this average is taken in practice) and in the limit where $\nu \to 0$ the scale by scale energy budget reduces to

$$\langle T_n\rangle \approx \frac{1}{2}\langle f_n u_n^* + f_n^* u_n\rangle. \tag{12}$$

The energy flux is defined as

$$\Pi_N = \sum_{n=1}^{N}\langle T_n\rangle. \tag{13}$$

Assuming power law solutions $u_n \sim k_n^\alpha$ and using equation (12), we get

$$\Pi_N = \frac{1}{2}\sum_{n=1}^{N}\langle f_n u_n^* + f_n^* u_n\rangle \sim \sum_{n=1}^{N} k_n^{\alpha+\beta} \tag{14}$$

because $f_n \sim k_n^\beta$. Note that we neglect the potential effects of the phases of the complex quantities f_n and u_n. It follows from 14 that Π_N is independent of N if $\alpha+\beta<0$. We might expect the N-independence of Π_N to imply Kolmogorov scaling and therefore $\alpha = -1/3$. Hence, for $\beta < 1/3$ we might predict $\alpha = -1/3$. For $\beta \ge 1/3$, however Π_N is not independent of N and Kolmogorov scaling cannot be expected to hold. Instead, we note from equation (10) that $T_n \sim k_n u_n^3$ and using also equation (12), $u_n \sim k_n^\alpha$ and $f_n \sim k_n^\beta$ we obtain

$$\alpha = \frac{\beta-1}{2}\,. \tag{15}$$

We have neglected the effect of the complex phases on the average values $\langle T_n\rangle$ and $\langle f_n u_n^*\rangle$ which could invalidate equation (15). We must in fact assume that these

complex phases do invalidate equation (15) in the range $\beta < 1/3$ where we expect $\alpha = -1/3$ because of the N-independence of Π_N in that range. Our numerical simulations reported in Section 5 indicate that they also invalidate equation (15) in the range $\beta > 1/3$ but not the qualitative conclusion that α is an increasing function of β in that range.

Note that equation (15) implies $\alpha = -1/3$ for $\beta = 1/3$ and that $-1/3 \leq \alpha < 0$ for $1/3 \leq \beta \leq 1$. All in all, our theory predicts that $\alpha = -1/3$ for $-2 < \beta \leq 1/3$ and that α increases above $-1/3$ as β increases in the range $1/3 < \beta < 1$. The line $\alpha + \beta = 0$ in the $\alpha - \beta$ plane is worth mentioning as it delineates between regions of N-dependent and N-independent energy flux. The average energy transfer $\langle T_n \rangle$ is an increasing function of k_n where $\alpha + \beta > 0$ and a decreasing function of k_n where $\alpha + \beta < 0$.

4.3 Amplitude and phase of the forcing

The fact that the coupling term in equation (1) gives, when multiplied by u_n, three terms all similar within prefactors and index displacements, means that the dynamics of the model are invariant with respect to the following phase transformation [16]:

$$u_n \rightarrow \mathrm{e}^{\mathrm{i}A} u_n \tag{16}$$

$$u_{n+1} \rightarrow \mathrm{e}^{\mathrm{i}(B-A)} u_{n+1} \tag{17}$$

$$u_{n+2} \rightarrow \mathrm{e}^{-\mathrm{i}B} u_{n+2} \tag{18}$$

where n modulo 3 is equal to 1 and where A and B are arbitrary constants.

Let us complement equation (2) as follows: $f_n = f\mathrm{e}^{\mathrm{i}\theta_f} k_n^\beta$ where f is real and positive and θ_f is the phase of the forcing. In this paper we experiment with various models for θ_f. First, we assume that the velocity phases are dominated by the forcing phase so that we should expect $u_n = |u_n|\mathrm{e}^{\mathrm{i}\theta_f}$. This assumption is reasonable because the arbitrary phases are constants of the phase transformation described above and can be chosen so that all the shells have approximately the same phase. Inserting $u_n = |u_n|\mathrm{e}^{\mathrm{i}\theta_f}$ in equation (1), dividing both sides by $\mathrm{e}^{\mathrm{i}\theta_f}$ and requiring all the terms to be real-valued yields $\mathrm{i}\mathrm{e}^{-\mathrm{i}3\theta_f} = \pm 1$. This implies that $\theta_f = \pi(\frac{1}{6} + \frac{1}{3}h), h = 1, ..., 6$ and, for simplicity's sake, we chose $h = 1$, thus making the forcing pure imaginary:

$$f_n = \mathrm{i} f k_n^\beta. \tag{19}$$

When not specified in the following sections the forcing is modelled as in equation (19) with f constant in time. However another case, referred to as **ST1**, is tested in this paper in which the forcing is also given by equation (19) but with f a real random number generated at every time step within the range $1 \times 10^{-3} < f < 10 \times 10^{-3}$ (it therefore oscillates around the usual value $f = 5 \times 10^{-3}$).

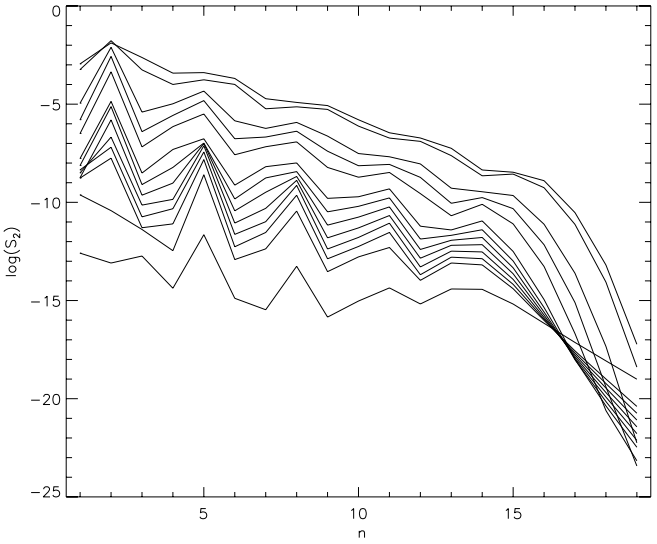

Fig. 2. The second order structure function *versus* the shell number, for different values of β, ranging from $\beta = -1/3$ (the steepest) to $\beta = 1$ (the shallowest). (The laboratory experiment limits us to $\beta < 1$ but the numerical simulations can be run for higher values of β too.) In all subsequent figures, numerically calculated scaling exponents are given with error bars which quantify the GOY model's oscillations around the power law fit.

Finally, three other different cases are tested here where the forcing phases are also chosen randomly: these cases are labeled **ST2**, **ST3** and **ST4**.

- **ST2** The forcing is defined as

$$f_n = Z f k_n^\beta \tag{20}$$

  where Z is a complex random number chosen among the six possible combinations $\pm\mathrm{i}$, $\pm\frac{\sqrt{(3)}}{2} \pm \frac{\mathrm{i}}{2}$ and $f = 5 \times 10^{-3}$.
- **ST3** The forcing is defined as

$$f_n = Z f k_n^\beta \tag{21}$$

  where Z is a complex random number chosen under the constraint $|Z| = 1$ and $f = 5 \times 10^{-3}$.
- **ST4** The forcing is defined as

$$f_n = Z f k_n^\beta \tag{22}$$

  where Z is a complex random number chosen among the six possible combinations $\pm\mathrm{i}$, $\pm\frac{\sqrt{(3)}}{2} \pm \frac{\mathrm{i}}{2}$ and f is a real random number chosen such that $1 \times 10^{-3} < f < 10 \times 10^{-3}$.

In all stochastic cases, the random number generation occurred at every time step.

5 Numerical results

It is customary in studies of shell-models to consider that the u_n characterise velocity differences across length-scales

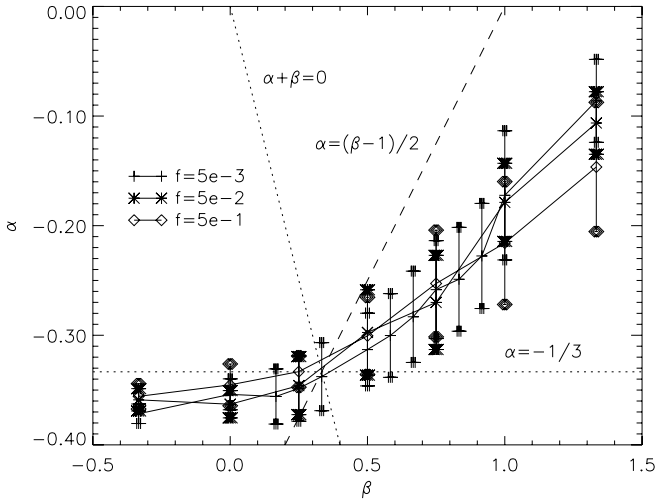

Fig. 3. α as a function of β for different strengths of forcing.

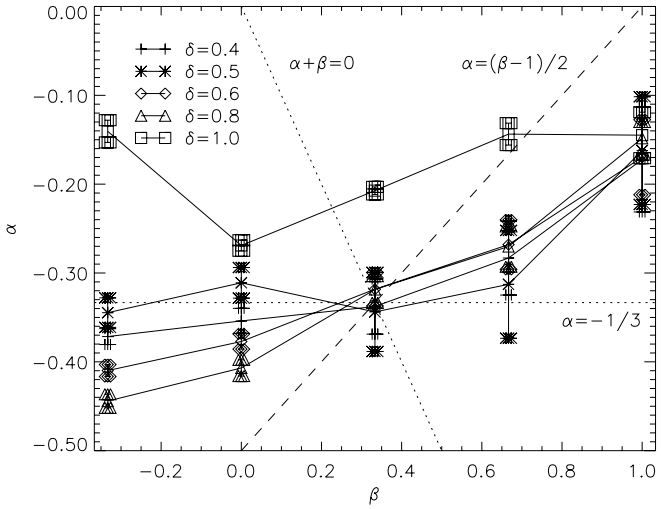

Fig. 4. α as a function of β for different values of δ.

$\ell_n \sim k_n^{-1}$ and from that calculate the surrogate structure function $\langle |u_n|^p \rangle$. These surrogate structure functions are assumed to scale with k_n^{-1} in the same way that $\langle |\delta u(l)|^p \rangle$ scale with l, *i.e.*

$$\langle |u_n|^p \rangle \sim k_n^{\xi_p} \tag{23}$$

where ξ_p are the same as the usual structure function scaling exponents but negative. Note that $\xi_1 = \alpha$.

The measurements are taken as follows: the simulation runs over a total of 5×10^5 time steps. During each time step the five first powers of $|u_n|$ are calculated and summed with their previous values. After the run these sums divided by the total number of time steps give $\langle |u_n|^p \rangle$ for different n and p and the exponents ξ_p are extracted using equation (23). We have checked the convergence of the exponents during the simulation, by calculating and recording these exponents 50 times uniformly spaced along the entire time-span of the simulations.

The measured values of $\xi_1 = \alpha$ and $\xi_2,\ \xi_3, ...$ are functions of β and will thus be denoted $\alpha(\beta),\ \xi_2(\beta),\ \xi_3(\beta)$ etc. Even though the scaling regions defining these exponents are generally the same for different values of the parameters of the model, it turns out that some variation occurs for extreme parameter-values. Because no simple mathematical criteria for choosing scaling regions exist, the regions are defined by visual inspection. As an example of the different scalings of a structure function with changing β, Figure 2 shows the second order structure function in the case where the forcing is fully deterministic with amplitude $f = 5 \times 10^{-3}$ and $\delta = 0.5$.

5.1 Relation between α and β

Figure 3 shows $\alpha(\beta)$ for three different values of f, where $f = 5 \times 10^{-3}$ is the standard value. As expected, the three $\alpha(\beta)$ curves overlap nicely especially for $\beta < 1$ (note that the laboratory experiments of [5] limit us to $\beta < 1$ anyway). We do find that α is constant for $\beta < -1/3$ but at a value slightly less than the predicted $-1/3$. This deviation from $-1/3$ may be an imprint of intermittent behaviour [11] the study of which is beyond the scope of this paper however. For $\beta = 1/3$ α is very close to the predicted $-1/3$ and α does indeed increase with β as predicted for $\beta > 1/3$ but not according to equation (15). The theory of Section 4 does therefore capture salient features of the β-dependence of α but not quantitative details which are presumably sensitive to phase dynamics.

If the requirement of helicity conservation is dropped, δ becomes a free parameter of the model. Because δ controls the amount of chaos in the dynamics of the model [17] we enquire how changes in δ may affect the scalings of the structure-functions. In Figure 4 we plot $\alpha(\beta)$ for standard forcing ($f = 5 \times 10^{-3}$), but for five different values of δ ranging from just above the onset of chaotic dynamics at $\delta = 0.4$ to a limit-value $\delta = 1.0$ where the turbulent nature of the shell-model dynamics have already been questioned [18]. We observe that, with the exception of $\delta = 1$, $\alpha = -1/3$ at $\beta = 1/3$ for all values $\delta = 0.4, 0.5, 0.6, 0.8$. Also, again with the exception of $\delta = 1$, α remains an increasing function of β albeit with some systematic δ-variability particularly at values of β smaller than 1/3 where $\alpha(\beta)$ tends towards $\alpha = -1/3$ as δ decreases.

6 Comparison with experiment

In their laboratory experiments, Queiros-Conde and Vassilicos [5] measured the exponents ξ_2 and ξ_3 as functions of D_f. For comparison ξ_2 is plotted in Figure 5 as a function of β for different strengths of forcing. No dependence on the amplitude of the forcing is observed and the behaviour of $\xi_2(\beta)$ resembles that of $2\alpha(\beta)$. The Kolmogorov value $\xi_2 = -2/3$ is obtained for $\beta = 1/3$, the value of β where T_n is independent of k_n. Note that $\xi_2 \approx -2/3$ for $\beta \leq -1/3$ indicating that ξ_2 remains unchanged by a rate of transfer of energy which decelerates with increasing k_n (implying an energy flux Π_N

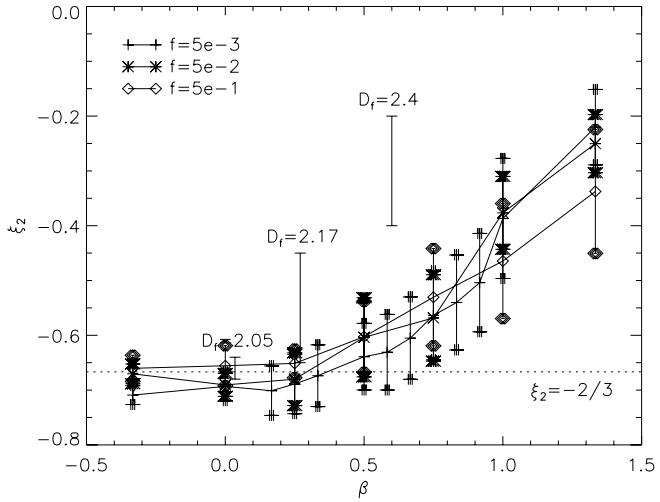

Fig. 5. ξ_2 as a function of β for different strengths of forcing with experimental values given (thicker bars) as a range of values (see explanation for this range of values in the first paragraph of Sect. 6).

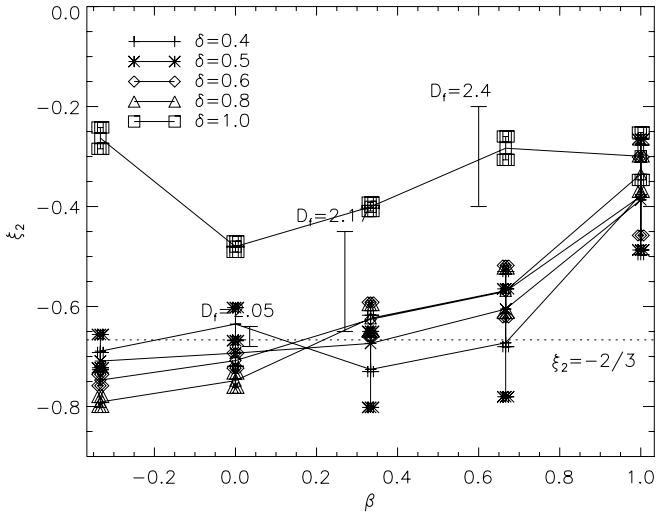

Fig. 6. ξ_2 as a function of β for different values of δ with experimental values given (thicker bars) as a range of values (see explanation for this range of values in the first paragraph of Sect. 6).

independent of N). It is when the rate of transfer of energy is forced to accelerate with increasing k_n that ξ_2 switches from the classical value $-2/3$ towards values larger than $-2/3$. This qualitative behaviour of $\xi_2(\beta)$ is confirmed by values of ξ_2 experimentally measured in the laboratory which are shown in Figure 5 with the symbol commonly used for error-bars (in the laboratory experiments of [5] the ratio of the largest length-scale to the smallest resolved length-scale of the turbulence is not more than 100 and as in many other turbulence experiments such a ratio did not prove sufficient for the existence of well defined power-laws; therefore the experimental results instead of featuring $S_p(r)$ plotted as a function of scale, present ξ_p plotted as a function of the scale. This explains the "error bars" in Figures 5 and 6: they do not represent an actual error but rather the range of values taken by the exponent ξ_p. In our shell-model, however, the ratio of outer to inner length-scales is larger than 10^5).

In Figure 6 we plot $\xi_2(\beta)$ for standard forcing but for five different values of δ. The conclusions to be drawn for $\xi_2(\beta)$ are broadly the same as those drawn for $\alpha(\beta)$ from Figure 4. Note also that the δ-variation of $\xi_2(\beta)$ does not improve the quantitative comparison between laboratory values and shell-model values of ξ_2. In fact, ξ_2 takes the Kolmogorov value $-2/3$ at $\beta = 1/3$ only for the standard value $\delta = 0.5$ where the GOY model is as close as possible to the Navier-Stokes equations because of helicity conservation.

In Figure 7 the value of the third order structure function scaling exponent ξ_3 is plotted as a function of β for different strengths of forcing: the behaviour of the function agrees qualitatively with the results of the experiment. In Figure 8 ξ_3 is plotted *versus* β for different values of δ. These two figures confirm and widen the conclusions already drawn from the previous figures.

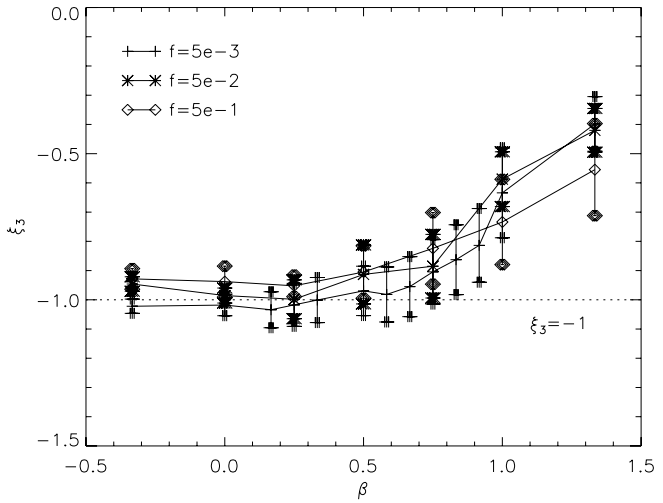

Fig. 7. ξ_3 as a function of β for different strengths of forcing.

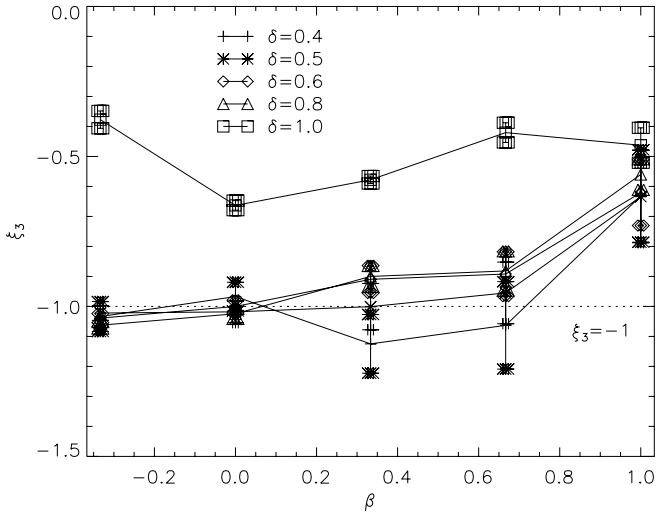

Fig. 8. ξ_3 as a function of β for different values of δ.

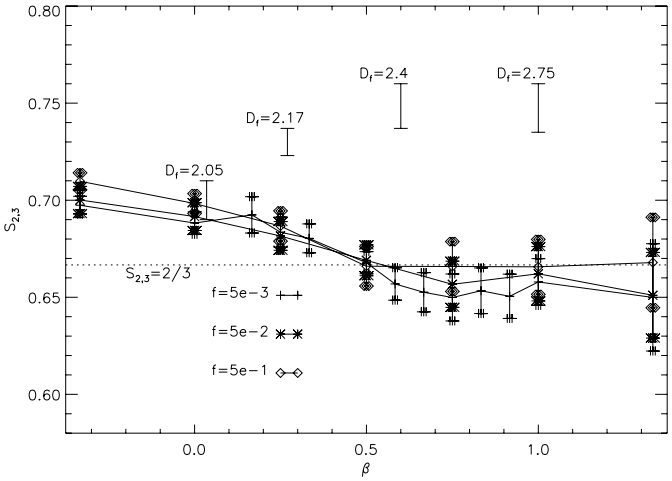

Fig. 9. $S_{2,3}$ as a function of β for different strengths of forcing with experimental values given (thicker bars) as a range of values (see explanation for this range of values in the first paragraph of Sect. 6).

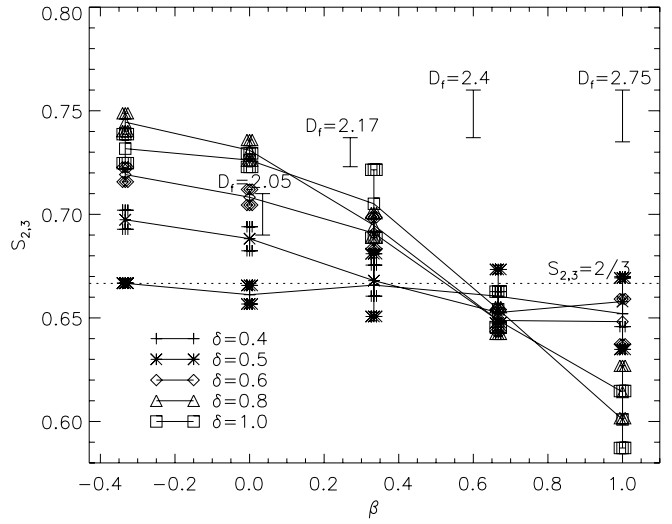

Fig. 10. $S_{2,3}$ as a function of β for different values of δ with experimental values given (thicker bars) as a range of values (see explanation for this range of values in the first paragraph of Sect. 6).

We apply now the extended self-similarity (ESS) way of plotting structure functions [14,19] and look for a scaling between the second and third order structure-function,

$$\langle |u_n|^2 \rangle \sim \langle |u_n|^3 \rangle^{S_{2,3}}. \tag{24}$$

The comparison between values of $S_{2,3}$ from the model and the laboratory experiments is shown in Figures 9 and 10 for different strengths of forcing and different values of δ. Contrary to ξ_2 and ξ_3 there is no qualitative agreement between the β-dependence of $S_{2,3}$ in the shell-model and that of $S_{2,3}$ in the laboratory experiment. Because $S_{2,3} = \xi_2/\xi_3$ this means that whereas ξ_3 decreases at a faster rate than ξ_2 with increasing D_f in the laboratory experiment, in the shell model ξ_3 decreases at a slower rate than ξ_2 with increasing D_f.

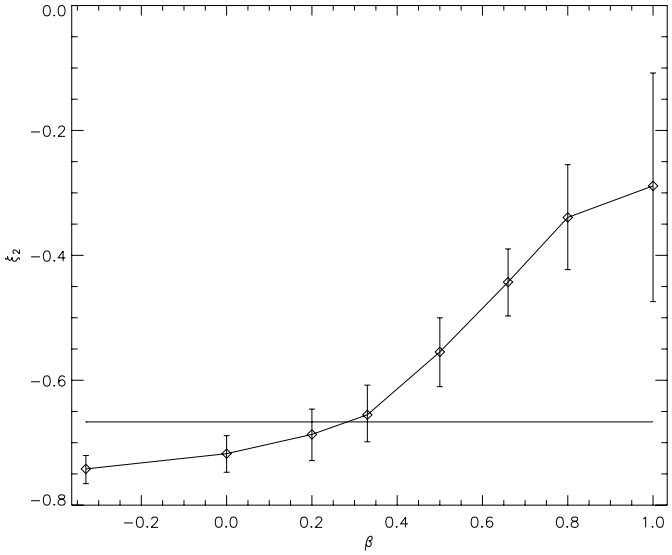

Fig. 11. ξ_2 as function of β for the stochastic case **ST1** with error bars. The horizontal line indicates Kolmogorov value of $-2/3$.

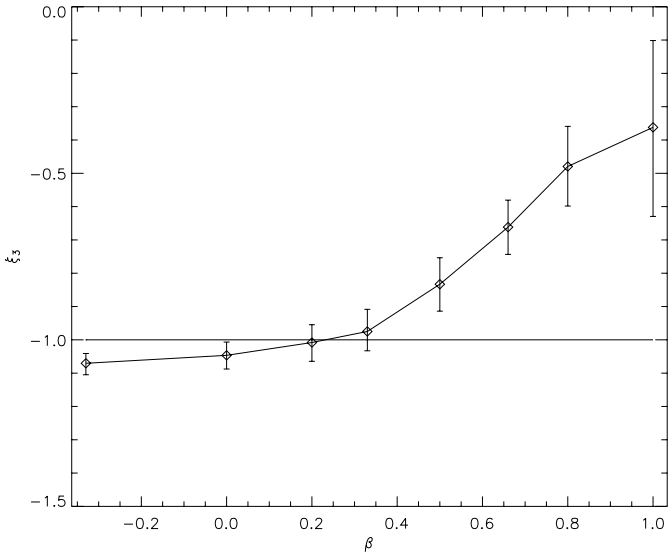

Fig. 12. ξ_3 as function of β for the stochastic case **ST1** with error bars. The horizontal line indicates Kolmogorov value of -1.

7 Dependence on forcing model

Figures 11 and 12 show the value of the exponent of the second and third order structure functions respectively for the case **ST1**: for low values of β, and in particular for $\beta = 1/3$, these results are in qualitative and quantitative agreement with the previous ones, it is not however the case for values $\beta \gg 1/3$ where the agreement is only qualitative. It might not be too surprising that such a disagreement occurs in that region because random fluctuations of the forcing amplitude are increased by a larger exponent of k_n. However it is harder to see why such disagreement should result in a consistently lower value of the exponent ξ_2.

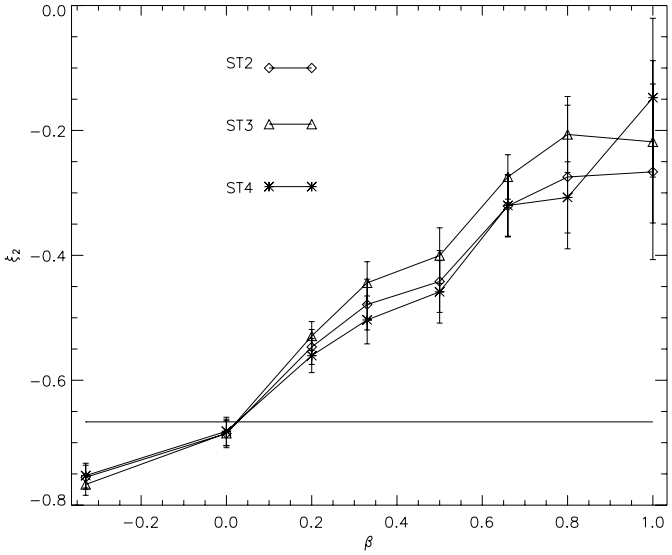

Fig. 13. ξ_2 as function of β for the stochastic cases **ST2**, **ST3**, **ST4** with error bars. The horizontal line indicates Kolmogorov value of $-2/3$.

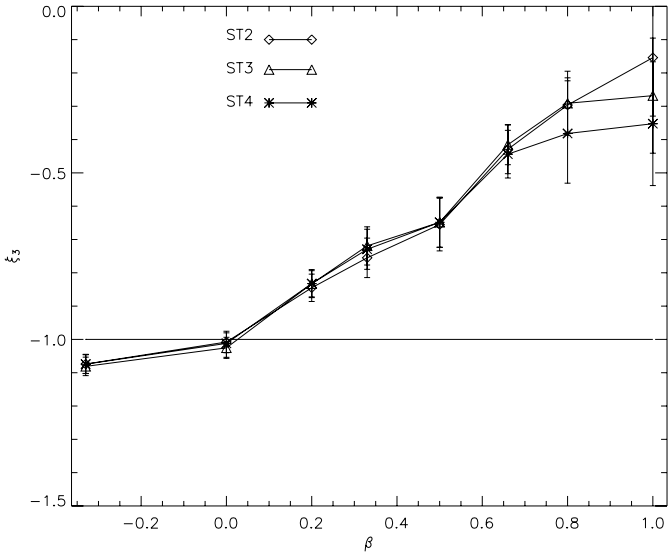

Fig. 14. ξ_3 as function of β for the stochastic cases **ST2**, **ST3**, **ST4** with error bars. The horizontal line indicates Kolmogorov value of -1.

Figures 13 and 14 are similar plots for the remaining cases where the forcing phases are random. The results remain qualitatively unchanged insofar as ξ_2 and ξ_3 remain increasing functions of β, but there are important quantitative differences. For example $\xi_2 = -2/3$ and $\xi_3 = -1$ are now achieved at a value of β significantly smaller than $1/3$ and rather close to 0. These quantitative differences are brought out more dramatically in plots of $S_{2,3}$ *versus* β (see Figs. 15 and 16) where they even imply a qualitative difference in behaviour from Figure 9 at values of β larger than 0.6.

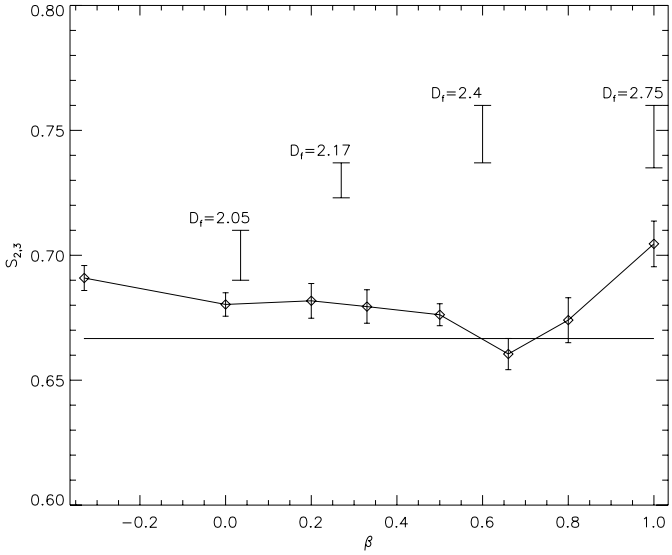

Fig. 15. $S_{2,3}$ as function of β for the stochastic cases **ST1** with error bars. The horizontal line indicates Kolmogorov value of $-2/3$.

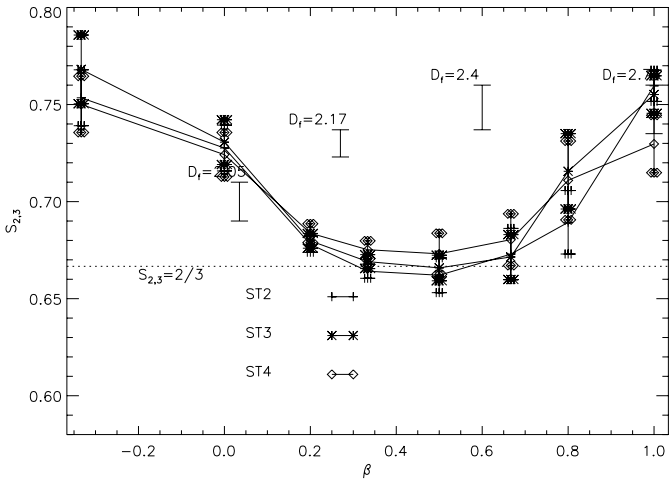

Fig. 16. $S_{2,3}$ as function of β for the stochastic cases **ST2**, **ST3**, **ST4** with error bars. The horizontal line indicates Kolmogorov value of $-2/3$.

8 Conclusion

In this paper we have developed a shell model of fractal-induced turbulence. The motivation for this work lies in a recent laboratory experiment [5] where turbulence was created by a fractal grid object (see Fig. 1) in a wind tunnel. In the shell model the fractal forcing is modelled by a power law forcing of the GOY equations (Eq. (1)) of the form

$$f_n \sim k_n^{\beta}. \tag{25}$$

A simple argument based on drag considerations suggests that β is an increasing function of the fractal dimension D_f of the fractal object. Reasoning on the scale-by-scale energy budget and energy flux, and assuming statistical stationarity and power-law solutions $u_n \sim k_n^{\alpha}$ leads

to $\alpha = -1/3$, $\xi_2 = -2/3$ and $\xi_3 = -1$ for $\beta \leq 1/3$ and to α, ξ_2 and ξ_3 being increasing functions of β for $\beta \geq 1/3$. Numerical integrations of the fractal forced shell-model equations support these conclusions for a variety of values of δ strictly smaller than 1. The critical value $\beta = 1/3$ is indeed observed when the phases of the fractal forcing are not random but not when they are random. We note that ξ_2 and ξ_3 are increasing functions of β (and therefore of D_f) in agreement with experimental results [5].

The results, in particular ESS, are sensitive to the modelling of the fractal forcing phases. It is possible to imagine the forcing phases in spectral space as corresponding to the shape of the fractal object in real space. Different fractal objects can be built with the same fractal scaling (and therefore same fractal forcing scaling $f_n \sim k_n^\beta$) but different fractal phases. The present study supports the idea that fractal forcing can alter turbulence scalings and dynamics, but also suggests that details of the fractal construction other than the fractal dimension can have measurable effects too. For example, fractal forcing with random phases can generate an increasing dependence of the ESS exponent ξ_2/ξ_3 on D_f, as indeed observed in the laboratory experiment of [5] but in a different range of D_f values (though the relation between β and D_f given in this paper might not be quantitatively accurate enough to compare these ranges). On the other hand, fractal forcing with constant phases produces a decreasing dependence of ξ_2/ξ_3 on D_f.

We have shown in Section 4 how scaling exponents can change as a result of the fractal forcing modifying energy flux by, in fact, accelerating it at smaller scales. Numerical and laboratory experiments with fractal forced turbulence provide, therefore, a new tool for the investigation of the dynamics, scaling and phases of turbulent flows. More laboratory research is needed with different fractal objects and a better understanding is also needed of the numerical modelling of the fractal forcing applied by different fractal objects.

We would like to thank one of the referees for very useful suggestions that have significantly improved the paper. We also acknowledge suggestions from and enlighting discussions with: Diego Queiros-Conde, Jean-François Pinton and Stephen D. Griffiths. We are grateful for financial support to the Royal Society and the ECTMR network on intermittency which made it possible for Fridolin Okkels to spend the period September 1999 to January 2000 in DAMTP, Cambridge, where a significant part of the research work reported in this paper was carried out.

References

1. E.A. Novikov, Prikl. Math. Mekh. **35**, 266 (1970)
2. J. Mandelbrot, J. Fluid Mech. **62**, 331 (1974)
3. U. Frisch, P.L. Sulem, M. Nelkin, J. Fluid Mech. **87**, 719 (1978)
4. T.S. Lundgren, Phys. Fluids **25**, 2193 (1982)
5. D. Queiros-Conde, J.C. Vassilicos, *Turbulent wakes of 3-D fractal grids*, in *Intermittency in turbulence flows*, edited by J.C. Vassilicos (Cambridge University Press, 2000)
6. R.H. Kraichnan, Phys. Rev. Lett. **72**, 1016 (1994)
7. E.B. Gledzer, Sov. Phys. Dokl. **18**, 216 (1973)
8. M. Yamada, K. Ohkitani, J. Phys. Soc. Jpn **56**, 4210 (1987); Prog. Theor. Phys. **79**, 1265 (1988)
9. L. Kadanoff, D. Lohse, J. Wang, R. Benzi, Phys. Fluids **7**, 617 (1995)
10. L. Biferale, A. Lambert, R. Lima, G. Paladin. Physica D **80**, 105 (1995)
11. T. Bohr, M.H. Jensen, G. Paladin, A. Vulpiani, *Dynamical systems approach to turbulence* (Cambridge University Press, Cambridge, 1999)
12. F. Okkels, Master thesis, CATS, University of Copenhagen, Denmark (1997)
13. L.F. Richardson, *Weather prediction by numerical process* (Cambridge University Press, Cambridge UK, 1922)
14. U. Frisch, *Turbulence: The legacy of A.N. Kolmogorov* (Cambridge University Press, 1995)
15. D. Pisarenko, L. Biferale, D Courvasier, U. Frisch, M. Vergassola, Phys. Fluids A **65**, 2533 (1993)
16. O. Gat, I. Procaccia, R. Zeitak, Phys. Rev. E, **51**, 1148 (1995)
17. J. Kockelkoren, F. Okkels, M.H. Jensen, J. Stat. Phys. (1998)
18. P.D. Ditlevsen, I.A. Mogensen, Phys. Rev. E **53**, 4785 (1996)
19. F. Benzi, S. Ciliberto, C. Tripiccione, C. Baudet, F. Massaioli, S. Succi, Phys. Rev. E **48**, R29 (1993)